ACS OMEGA

Open Access

http://pubs.acs.org/journal/acsodf

Article

Evaluation of Mono and Bimetallic Ferrocene-Based 1,2,3-Triazolyl Compounds as Burning Rate Catalysts for Solid Rocket Motor

Cristian Valdebenito, José Gaete, Claudio Osorio, Yuvaraja Dibdalli, Ángel Norambuena, Nathalie Lecaros, Cristian Carrasco, Héctor Reyes, Gabriel Abarca,* and Cesar Morales-Verdejo*

Cite This: *ACS Omega* 2023, 8, 35242−35255

Read Online

ACCESS | Metrics & More | Article Recommendations | Supporting Information

ABSTRACT: We reported mono and bimetallic ferrocene-based 1,2,3-triazolyl compounds as potential burning rate catalysts in their neutral and ionic forms. All complexes reported here were characterized using ^{1}H and ^{13}C NMR, elemental analysis, and Mössbauer spectroscopy, which was performed for neutral and oxide compounds. The complexes present quasireversible redox potentials with higher oxidative ability than ferrocene and catocene under the same conditions. The complexes were tested as catalysts on the thermal decomposition of ammonium perchlorate (AP) and examined by a differential scanning calorimetry technique to gain further knowledge about their catalytic behavior. Compound **1** causes a decrease of the high-temperature decomposition (HTD) of AP positively, decreasing the decomposition temperature of AP to 345 °C and consequently increasing the energy release to 1939 $J \cdot g^{-1}$. We took the residues from the pans after testing from the DSC to elucidate the underlying reaction pathways. We obtained the size of the nanostructures formed after thermal decomposition of AP determined by the TEM technique. The diameter and size distribution of iron oxide nanoparticles formed depend on the alkyl sidechain of the triazolium ring, which induces the formation of nanoparticles with a double diameter and size distribution compared to their neutral analogues, suggesting that the possible intermediate for the mechanism degradation of AP by ferrocene derivatives is nanoscale Fe_2O_3 or similar oxides.

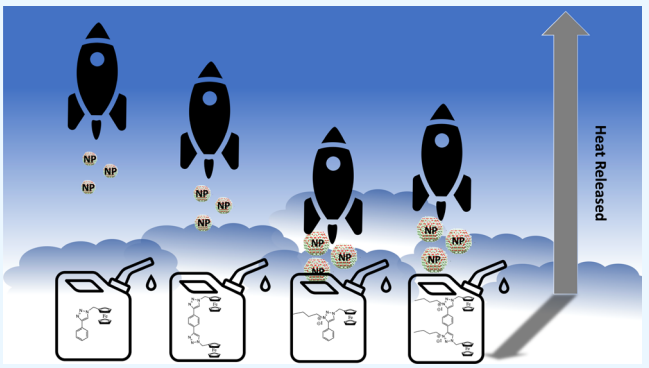

1. INTRODUCTION

Rocket technology research has been a subject of increasing interest in recent years due to its wide-ranging aerospace applications.[1,2] Propulsion is the core component of aerospace technology, and propellants are the most critical ingredients used in rockets, aircraft, missiles, and other space technologies to provide the driving force. Therefore, various propellants must be developed to meet the specific requirements of different applications.[3−5]

Modern composite solid propellants (CSPs) are typically made up of a mixture of chemical ingredients, including isophorone diisocyanate (IPDI, curative), hydroxyl-terminated polybutadiene (HTPB, prepolymer), ammonium perchlorate (AP, oxidizer), a catalyst, and other additives.[6] The high-performance solid propellant requires a regular combustion rate, a low-pressure index, and high heat release. AP, a vital oxidizer, is widely used in CSPs, and its decomposition directly determines propellant performance.[3,7]

Controlling the AP decomposition process is crucial in obtaining as much powerful impetus as possible.[6,8] Therefore, considerable efforts have been made to modify the decomposition process of AP in two ways. The first method involves preparing superfine AP crystals to enhance combustion behavior. The second method involves studying and designing combustion catalysts currently applied to modern CSPs.[9]

Several studies have focused on synthesizing combustion catalysts to improve CSPs' burning rate and antimigration ability.[9] These catalysts can be classified into four categories: transition metal oxides,[10,11] nanoparticles,[12−16] transition metal complexes,[17−20] and ferrocene (Fc)-based compounds.[7,9,21−27] Transition metal oxides are inexpensive and simple to produce but have less worth in combustion. Nanoparticles have the advantage of being easier to transfer electrons and significantly reducing the decomposition temperature and activation energy for AP.[12,13] However, they are prone to aggregate and preferentially adsorbed on components during mixing, resulting in less dispersion of nano-Fe_2O_3 particles and heat release of AP.[9] Fc-based

Received: July 12, 2023
Accepted: September 1, 2023
Published: September 14, 2023

compounds, with their excellent redox and electrocatalytic properties, have attracted much attention for their potential in the research of CSPs.[28] It should be noted, though, that these ferrocene derivatives exhibit significant volatility during the propellant's curing process, and over extended periods of storage, there is noticeable migration toward the surface of the propellant columns.[9,28]

Researchers have tried overcoming the high-migration and volatility problems with ferrocene-based burn rate (BR) catalysts in recent decades. These efforts involved diverse approaches such as developing ferrocenyl group-grafted polymers[29,30] and dendrimers,[22,31] introducing concepts of ionic coordination compounds[32] and energetic ionic ferrocene,[33,34] besides increasing the molecular weights of ferrocene-based BR catalysts.[35−37] In the last ten years, Zhang and co-workers have utilized the concept of energetic ionic compounds to develop energetic ionic ferrocenyl compounds to tackle high-migration problems. Recently, Zhang's group has published the synthesis of various nitrogen-rich N-heterocyclic ferrocene-functionalized pyrazole and 1,2,3-triazolyl compounds and their effects on the thermal stability and combustion properties of composite propellants, showing exceptional antimigration ability and electrochemical properties, confirming that high nitrogen content in a ferrocenyl derivative improves its catalytic combustion performance in the thermal degradation of AP.[25,38]

On the other hand, despite a large amount of published information on ferrocene derivatives as burn rate catalysts, the decomposition mechanism remains challenging to explain due to its redox complexity. Some efforts have been made through different methods, such as FT-IR in real time, where it is possible to observe the products generated by the thermal decomposition of AP.[39] Until now, the accepted intermediates for the mechanism degradation of AP by ferrocene derivatives are iron oxide nanoparticles, which are formed when the cyclopentadienyl ligand is cleaved from the iron atom and this is oxidized to nano-Fe_2O_3 in situ, which acts as a newly formed catalyst to catalyze AP's decomposition further. However, to our knowledge, no concrete evidence of this formation has been presented.

This work provides fundamental evidence for forming iron oxide nanoparticles into the mechanistic of the thermal decomposition of ammonium perchlorate using ferrocenyl compounds derived from the 1,2,3-triazolyl ligand.

2. EXPERIMENTAL SECTION

2.1. General Information of the Catalysts. All manipulations were carried out under a pure nitrogen atmosphere by using a vacuum atmosphere dry box equipped with a Model HE 493 Dri-Train cleaner or with the use of a vacuum line by using standard Schlenk tube techniques.

Reagent-grade solvents were distilled under an atmosphere of nitrogen from sodium benzophenone for *N*,*N*-dimethylformamide (DMF), acetonitrile, dichloromethane, toluene, petroleum ether, and THF (previously distilled from $AlLiH_4$) and from P_2O_5 for acetonitrile and dichloromethane.[40]

The synthesis of the following compounds has been reported previously: azidomethyl ferrocene [Fc-CH_2-N_3][41] and 1-(ferrocenylmethyl)-4-phenyl-1,2,3-triazole (**1**).[42] Ferrocene, phenylacetylene, 1,4-diethynylbenzene, and sodium ascorbate (purchased from Aldrich, Fc). Analytically pure grade AP with a particle size of 200 μm was purchased from SNPE Propulsion, Groupe SNPE.

Elemental analyses (C and H) were made with a Fissions EA 1108 microanalyzer. ^{1}H and ^{13}C NMR spectra were recorded on Bruker AC-400 and Bruker AC-200P spectrometers. Chemical shifts were reported in ppm relative to residual solvents and were assigned using 2D NMR tools. All peaks reported were singlets unless otherwise specified. Melting points of recrystallized compounds were measured with a standard Leitz microscope or a Stuart Melting Point SMP3 apparatus. Mössbauer spectra were obtained using a constant acceleration Mössbauer spectrometer with a ^{57}Co/Rh source. The source was moved via triangular velocity waveform, and the γ counts were collected in a 512 multichannel analyzer. The data were folded, plotted, and fitted by a computer procedure. Velocity calibration was performed using 25 lm thick metallic Fe foil. The Mössbauer spectral parameters are given relative to this standard at room temperature. Mössbauer analyses were carried out at the ICMAB-CSIC. Fourier transform infrared spectroscopy (FT-IR) spectra were measured using a JASCO FT-IR 4100 spectrometer in the 5−4000 cm^{-1} frequency range.

2.2. Synthesis Compounds. *2.2.1. [(Cp_2Fe)-Tr-Bz-But][I] (**1-IL**).* 1-(Ferrocenylmethyl)-4-phenyl-1,2,3-triazole (**1**) (0.340 g, 1 mmol) was added portion wise to a solution of iodobutane (0.275 g, 170 μL, 1.5 mmol) in acetonitrile (25 mL) and heated to reflux for 24 h. After being cooled at room temperature, the reaction mixture was verted on H_2O (50 mL) and extracted with dichloromethane (3 × 50 mL). The organic extract was evaporated to dryness in vacuo, obtaining a dark oil stable to air. Yield: 0.430 g (80%). Yield. M.p.: 119 °C.

Anal. Calc. for $C_{24}H_{28}N_3FeI$ (543.75): C, 53.26; H, 5.21; N 7.76. Found: C, 53.15; H, 5.35; N, 7.68.

FT-IR: ν = 3103 w, 2961 w, 1615 s, 1456 s, 1411 m, 1103 cm^{-1}.

^{1}H NMR (400 MHz, chloroform-*d*) δ 8.74 (s, 1H), 7.73 (dd, 5H), 4.55 (m, 2H), 4.43 (m, 2H), 4.09 (m, 2H), 3.30 (m, 2H), 3.16 (s, 5H), 2.10 (dd, 2H), 2.00 (dd, 2H), 0.99 (t, 3H).

^{13}C NMR (101 MHz, chloroform-*d*) δ 170.07, 143.12, 132.18, 129.98, 129.30, 55.03, 52.23, 39.38, 31.65, 31.11, 20.08, 13.64.

*2.2.2. [(Cp_2Fe)-Tr-Bz][BF_4] (**1+**).* 1-(Ferrocenylmethyl)-4-phenyl-1,2,3-triazole (**1**) (0.100 g, 0.29 mmol) was dissolved in 20 mL of THF, and the solution was added to $[FeCp_2]^+[BF4]^-$ (0.079 g, 0.28 mmol). Subsequently, the mixture was stirred at room temperature for 4 h, resulting in a precipitate formation. The mixture was filtered, and the insoluble material was washed with petroleum ether to remove all the ferrocene and dried under vacuum to obtain a stable compound to air dark red dust. Yield: 0.085 g (68.4%).

Anal. Calc. for $C_{19}H_{17}N_3FeBF_4$ (430.01): C, 53.07; H, 3.98; N, 9.77. Found: C, 53.18; H, 3.95; N, 9.69.

FT-IR: ν = 3093 w, 2961 w, 1617 s, 1445 s, 1421 m, 1110 cm^{-1}.

*2.2.3. [(Cp_2Fe)$_2$-Tr_2-Bz] (**2**).* 1,4-Diethynylbencene (0.200 g; 1.59 mmol) and azidomethyl ferrocene (0.767 g; 3.18 mmol) were dissolved in a mixture of DMF (20 mL) and H_2O (5 mL), and then, $CuSO_4{\cdot}5H_2O$ (0.040 g; 0.16 mmol) and sodium ascorbate (0.125 g; 0.63 mmol) were added, maintaining the system under vigorous stirring for 48 h at room temperature. Subsequently, the mixture was poured into 100 mL of H_2O, and the crude product was filtered. Finally, the product was boiled and filtered in hot ethanol, obtaining a pale-yellow solid. Yield 0.52 g (54%). M.p.: 201 °C

https://doi.org/10.1021/acsomega.3c04996
ACS Omega 2023, 8, 35242−35255

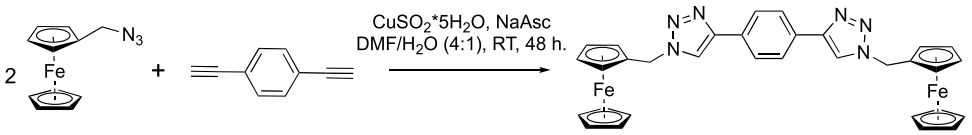

Figure 1. Synthetic pathway of ferrocenyl compound **2** derived from 1,2,3-triazolyl.

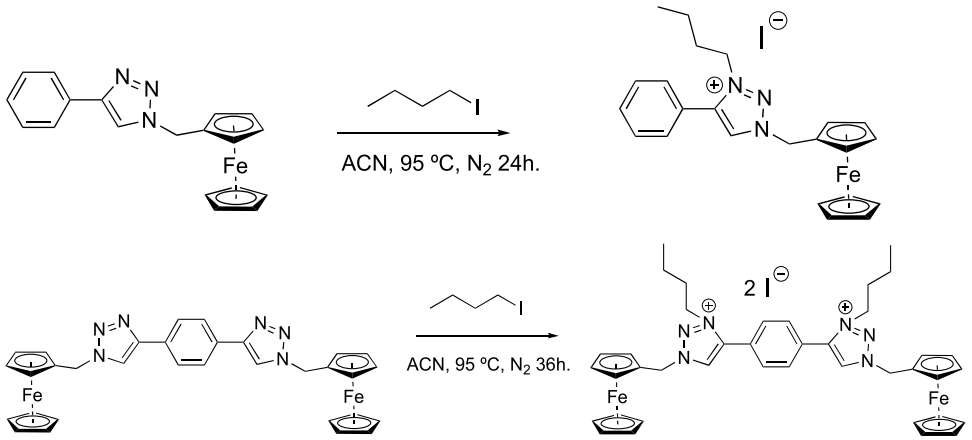

Figure 2. Synthetic pathway of ionic liquid ferrocenyl compounds **1-IL** and **2-IL** derived from 1,2,3-triazolyl.

Anal. Calc. for $C_{32}H_{28}N_6Fe_2$ (608.31): C, 63.18; H, 4.64; N, 13.82. Found: C, 63.07; H, 4.70; N, 13.67.

FT-IR: ν = 3090 w, 2977 w, 1669 s, 1456 s, 1410 m, 1105 cm^{-1}.

^{1}H NMR (400 MHz, DMSO-d_6) δ 8.50 (s, 2H), 7.81 (s, 4H), 5.27 (s, 4H), 4.32 (m, 4H), 4.13 (s, 10H), 4.12 (s, 4H).

^{13}C NMR / not found

*2.2.4. [$(Cp_2Fe)_2$-Tr_2-Bz-But][I_2] (**2-IL**).* Bis-(1-methylferrocenyl-4-fenil)-1H-1,2,3-triazole (0.500 g, 0.83 mmol) was added portion wise to a solution of iodobutane (0.380 g, 235 μL, 2.0 mmol) in acetonitrile (30 mL) and heated to reflux for 36 h. After being cooled at room temperature, the reaction mixture was verted on H_2O (50 mL) and extracted with dichloromethane (3 × 50 mL). The organic extract was evaporated to dryness in vacuo, obtaining a dark oil. Yield: 0.459 g (55%). M.p.: −17 °C

Anal. Calc. for $C_{42}H_{50}N_6Fe_2I_2$ (1009.5): C, 50.23; H, 5.02; N, 8.37. Found: C, 50.15; H, 5.18; N, 8.26.

FT-IR: ν = 3094 w, 2964 w, 1664 s, 1461 s, 1406 m, 1092 cm^{-1}.

^{1}H NMR (400 MHz, chloroform-*d*) δ 8.89 (s, 2H), 8.01 (s, 4H), 4.73 (m, 4H), 4.64 (m, 4H), 4.06 (m, 4H), 3.29 (m, 4H), 3.17 (s, 10H), 2.12 (m, 4H), 2.09 (m, 4H), 1.30 (t, 6H).

^{13}C NMR (101 MHz, chloroform-*d*) δ 170.17, 141.76, 131.79, 125.07, 55.10, 54.44−53.55 (m), 53.04, 39.39, 31.63, 23.45, 20.02, 13.76.

*2.2.5. [$(Cp_2Fe)_2$-Tr_2-Bz][BF_4] (**2+**).* Complex **2** (0.100 g, 0.164 mmol) was dissolved in 20 mL of THF, and the solution was added to $[FeCp_2]^+[BF4]^-$ (0.042 g, 0.156 mmol). Subsequently, the mixture was stirred at room temperature for 4 h, resulting in a precipitate formation. The mixture was filtered, and the insoluble material was washed with petroleum ether to remove all the ferrocene and dried under vacuum to obtain a stable compound to air dark red dust. Yield: 0.089 g (78.1%).

Anal. Calc. for $C_{32}H_{28}N_6Fe_2BF_4$ (695.11): C, 55.29; H, 4.06; N 12.09. Found: C, 55.21; H, 4.17; N, 12.09.

FT-IR: ν = 3105 w, 2958 w, 1627 s, 1458 s, 1407 m, 1089 cm^{-1}.

2.3. Thermal Analysis. Differential scanning calorimetry (DSC) analyses were performed on a DSC 822e METTLER TOLEDO instrument at a heating rate of 5 °C·min^{-1} under nitrogen in the 80−500 °C range. To investigate the catalytic performance of the compounds derived from 1,2,3-triazolyl for the thermal decomposition of AP, specific amounts of the complexes and AP were physically mixed and ground in a certain weight ratio for DSC analysis. For DSC analysis, 40 μL aluminum pans were used without a pin on the bottom for the measurement.

2.4. Electrochemical Measurements. The electrochemical properties of the samples were measured at room temperature using a Voltalab (PGZ100) potentiostat electrochemical workstation. A conventional three-compartment cell was utilized, where a platinum disk electrode with a diameter of 2 mm served as the working electrode, and a coiled Pt wire of a large area was used as the counter electrode. A sintered glass frit separated the counter electrode from the electrolytic solution. Before each experiment, the working electrode was polished to a mirror finish using an aqueous alumina slurry with particle sizes of 0.3 and 0.05 μm on microcloth pads, rinsed with water, and dried. All potentials were referred to an Ag/AgCl (KCl, 1.0 M) electrode. The working solution was purged with high-purity argon for 15 min before each experiment, and a lower flow was maintained over the solution during the measurements. The supporting electrolyte, tetrabutylammonium tetrafluoroborate $[Bu_4N][BF_4]$, was dried at 110 °C and kept in a dryer until use. Cyclic voltammetry measurements were carried out using anhydrous dimethyl sulfoxide (DMSO) with a concentration of 0.01 M $Bu_4N{\cdot}BF_4$ and 5 mM analyte at a scan rate of 100 mV·s^{-1}.

3. RESULTS AND DISCUSSION

The versatile nature of ferrocene-based 1,2,3-triazolyl compounds also allows for structural modification and functionalization, enabling the design of tailor-made molecules with

https://doi.org/10.1021/acsomega.3c04996
ACS Omega 2023, 8, 35242−35255

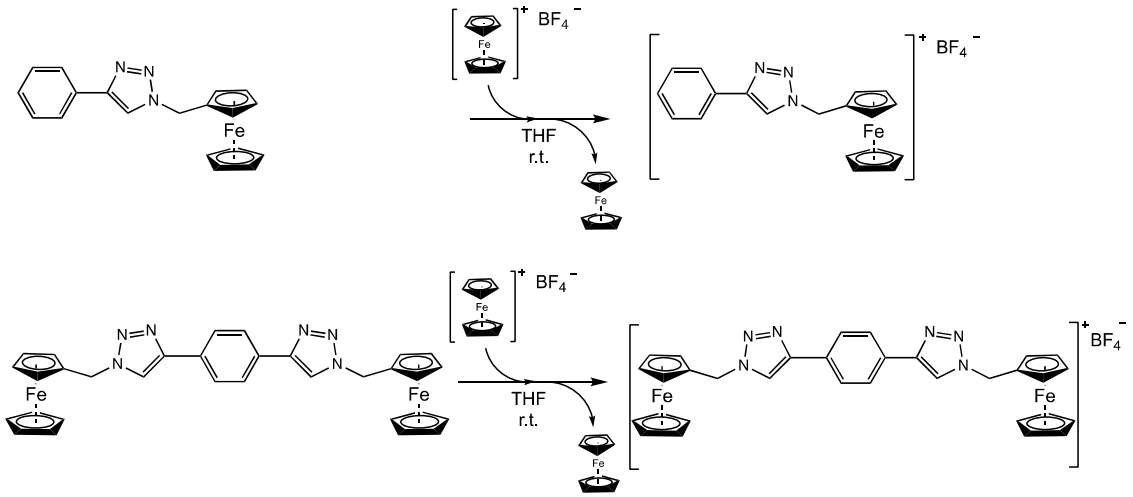

Figure 3. Synthetic pathway of oxidized ferrocenyl compounds **1**+ and **2**+ derived from 1,2,3-triazolyl.

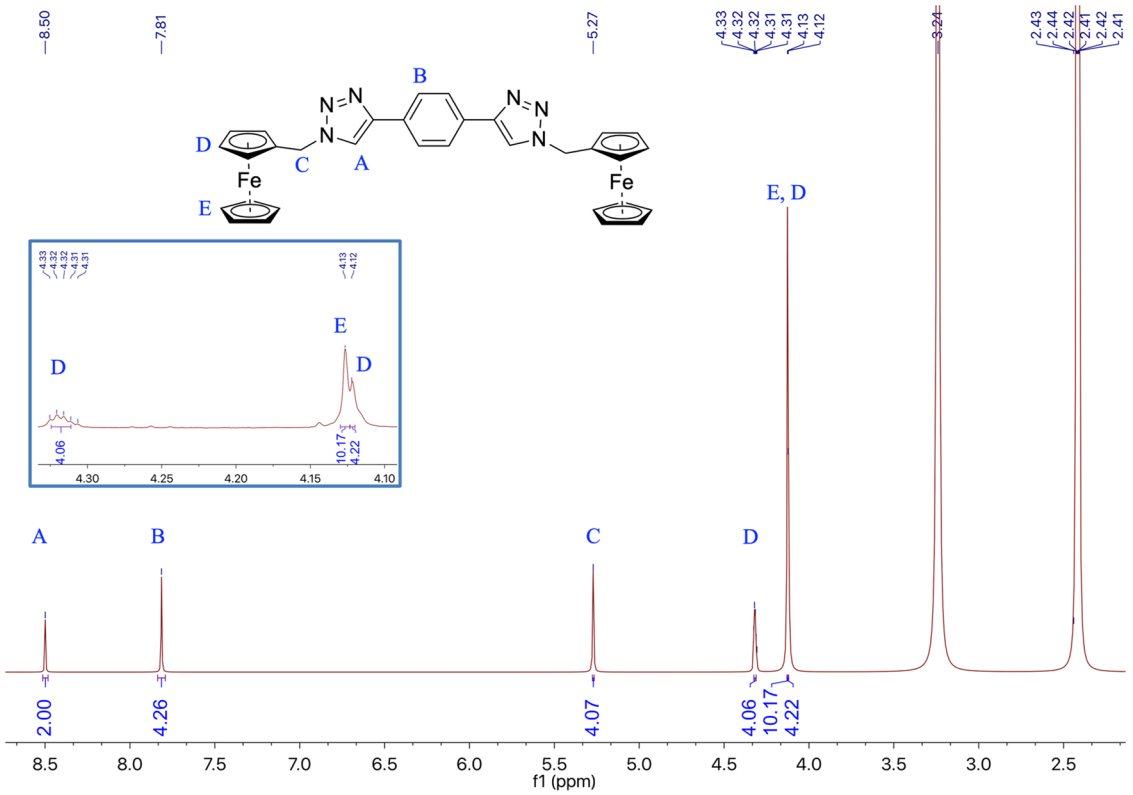

Figure 4. ^{1}H NMR spectrum of binuclear complex **2**, [$(Cp_2Fe)_2$-Tr_2-Bz], in DMSO-d_6.

desired properties. By tuning the substituents on both the ferrocene and triazole moieties, it is possible to modulate these compounds' electronic, steric, and physicochemical properties, further expanding their potential applications.[43−45]

The mono- and bimetallic complexes' neutral, oxidized, and ionic forms were characterized through NMR, FT-IR, and Mossbauer spectroscopies (neutral and oxidized compounds), which will be detailed below. Compounds **1** and **2** were synthesized by click reaction, obtaining yields of 70 and 54%, respectively (Figure 1). The compounds **1-IL** and **2-IL** were synthesized by N-alkylation reaction with a solution of iodobutane with yields of 80 and 55%, respectively (Figure 2). Finally, the oxidation reaction was carried out at room temperature with one equivalent of ferrocenium, obtaining a 68 and 78% yield for compounds **1**+ and **2**+, respectively (Figure 3).

Compounds **1** and **2** are soluble in DMSO and less soluble in dichloromethane; ionic compounds are utterly soluble in polar solvents.

Considering that the ferrocene-type complexes have been reported to be effective catalysts on the thermal decomposition of AP, this prompted us to test the activity of the complexes **1**, **2**, **1-IL**, and **2-IL** as burning rate catalysts in comparison with ferrocene (Fc) and catocene (Cat), to understand the role of the redox potential in the thermal decomposition of AP.

3.1. NMR Analysis. The spectroscopical analyses of each of the nuclei were carried out. Compound **2** can be observed in the ^{1}H NMR spectrum (Figure 4), which shows signals at δ

https://doi.org/10.1021/acsomega.3c04996
ACS Omega 2023, 8, 35242−35255

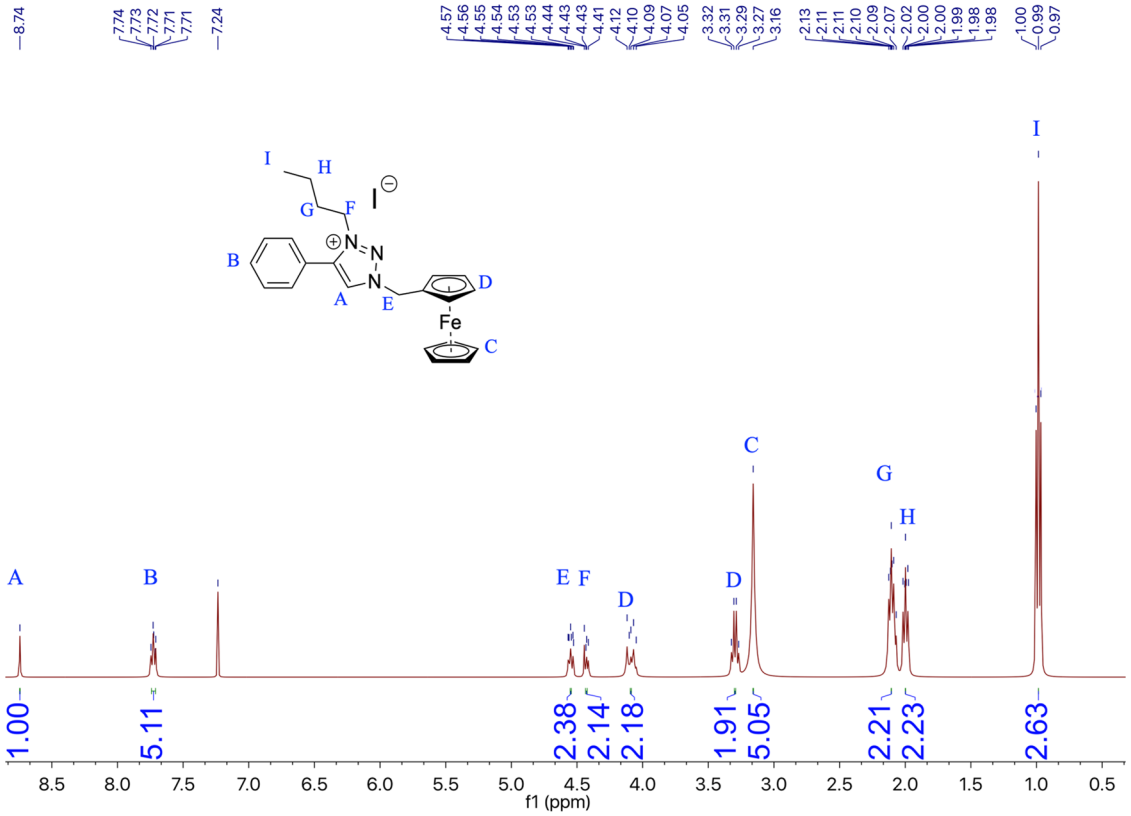

Figure 5. ^{1}H NMR spectrum of monometallic complex **1-IL** [(Cp_2Fe)-Tr-Bz-But][I] in chloroform-*d*.

8.50 ppm corresponding to the triazolyl group proton and 7.81 ppm, which can be attributed to the aromatic protons. The sign at δ 5.27 ppm corresponds to the two methylene protons. The signals at δ 4.32−4.31, 413, and 4.12 ppm correspond to protons of the ferrocene moiety. Unfortunately, ^{13}C NMR spectrum is not given due to the low solubility of compound **2** in deuterated DMSO solvent (Figure S1).

The ^{1}H NMR spectrum (Figure 5) of the compound **1-IL**, the same way as compound **1** previously informed,[46] shows signals at δ 8.77 and 7.67−7.56 ppm, which can be attributed to the protons of the triazolyl and the phenyl ring, respectively. The most notable signals indicating N-alkylation corresponding to the butyl group appear at δ 4.74, 4.53, 2.10, and 0.99 ppm, corresponding to the butyl group's protons. The signal at δ 3.16 ppm corresponds to the protons on the Cp ring of the ferrocene moiety. The most notable signals in the ^{13}C NMR spectrum at δ 31.11, 20.08, and 13.64 ppm correspond to the carbons of the butyl group (Figure S2). According to the ^{1}H NMR (Figure S3) data given for compound **2-IL**, like its mononuclear counterpart, the outstanding signals are at δ 4.72, 2.11, 1.99, and 1.31 ppm corresponding to the protons in the butane chain. In the case of the ^{13}C NMR spectrum (Figure S4), the signals standout at 31.63, 23.45, 20.02, and 13.76 ppm, corresponding to the carbons belonging to the butyl groups.

3.2. FT-IR Analysis. Table 1 summarizes the main stretching frequencies for compounds **1**, **2**, **1-IL**, and **2-IL** here reported (Figures S7−S9). For compounds **1** and **2**, the peak at 3069 cm^{-1} is assigned to C−H stretching vibrations of the aromatic ring (phenyl and ferrocene moiety[47]), and the peak at 2923 cm^{-1} is assigned to C−H stretching vibrations of the methylene group. The peak at 1615 cm^{-1} is assigned to N═N stretching vibrations of the triazolyl moiety.[48]

Table 1. Main Stretching Frequencies of FT-IR Spectra

complex	wavenumber (cm^{-1})	
1	C−$H_{Aromatic}$	3092
	C−$H_{Aliphatic}$	2961
	N−$N_{Triazolyl}$	1615
2	C−$H_{Aromatic}$	3090
	C−$H_{Aliphatic}$	2977
	N−$N_{Triazolyl}$	1669
1-IL	C−$H_{Aromatic}$	3103
	C−$H_{Aliphatic}$	2961
	N−$N_{Triazolyl}$	1615
2-IL	C−$H_{Aromatic}$	3094
	C−$H_{Aliphatic}$	2964
	N−$N_{Triazolyl}$	1664

The most remarkable is that after the N-alkylation reaction was carried out for compounds **1** and **2**, the stretching signal assigned to C−H at 2961 and 2964 cm^{-1} is observed due to the presence of butyl groups (Figures 6 and S9).

3.3. Redox Properties. The redox properties of all of the complexes in anhydrous DMSO solution were investigated by cyclic voltammetry to evaluate their oxidation ability and to understand the electrochemical reaction mechanism.

Table 2 summarizes the oxidation potentials of anhydrous DMSO solution reported with Ag/AgCl as the reference electrode. Compounds **1**, **2**, **1-IL**, and **2-IL** exhibited one quasireversible oxidation peak, associated with the oxidation of the iron center (Fe^{+2}/Fe^{+3}) in each complex, as has been observed by other authors[24,43,45] (Figure 7).

https://doi.org/10.1021/acsomega.3c04996
ACS Omega 2023, 8, 35242−35255

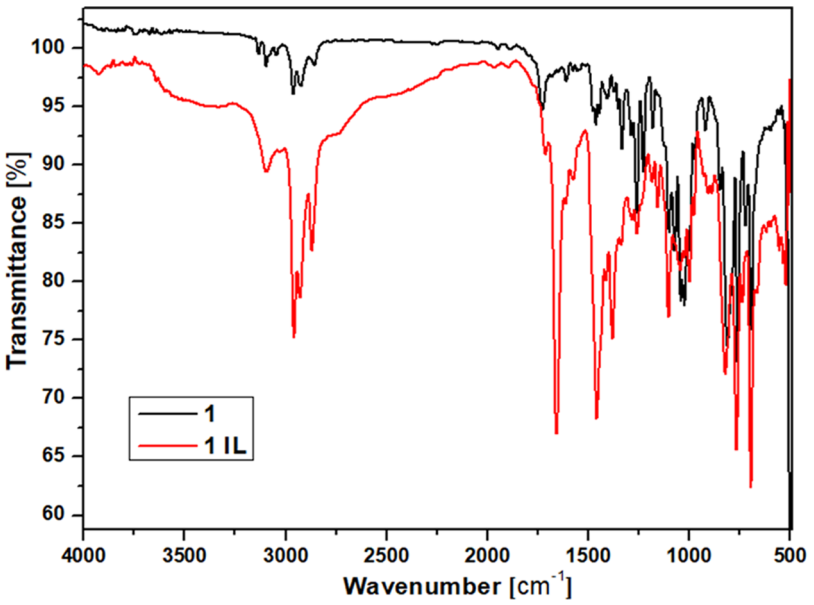

Figure 6. FT-IR spectra of compounds **1** and **1-IL**.

Table 2. Oxidation Potentials for Ferrocene (Fc), Catocene (Cat), and Complexes 1, 2, 1-IL, and 2-IL (mV vs Ag/AgCl)[a]

complexes	$E°(0/1+)$	$E°(1+/2+)$	$\Delta E_{1/2}$
1	−489		
2	−378		
1-IL	−454		
2-IL	577		
Fc	500		
Cat	346	498	152

[a] $\Delta E_{1/2}$ is the difference between the first and second oxidation potentials.

The oxidation potential of a compound can provide information about its ability to undergo oxidation reactions related to the catalytic effect on the thermal decomposition of AP. Compounds with lower oxidation potentials are easier to oxidize, while those with higher oxidation potentials are more difficult to oxidize.

If we compare the oxidation potentials shown above, it is possible to observe that compound **2-IL** has the highest oxidation potential at 577 mV, indicating that it is the most difficult to oxidize, similar to the electrochemical behavior of ferrocene with an oxidation potential of 500 mV, which is also relatively high. This value of complex **2-IL** suggests that due to the solid electron-withdrawing capacity of both quaternized triazoles, the electron density in both ferrocene moieties decreases and is not easily oxidized. The redox potential of this compound is higher than those of the compounds **1**, **2**, **1-IL**, and catocene, indicating that this compound has a stronger antioxidant capacity.

On the other hand, compounds **1** and **1-IL** have oxidation potentials of −489 and −454 mV, respectively, which indicates that they are relatively easy to oxidize. Compound **2** has an oxidation potential of −378 mV, higher than those of compounds **1** and **1-IL**, suggesting the ability to withdraw electrons from both triazole fragments.

Overall, the oxidation potential can provide helpful information about the reactivity and properties of the compounds and can be used to compare their relative stability toward oxidation reactions.

3.4. Mössbauer Analysis. The Mössbauer spectra of the neutral and oxidized complexes were acquired at room temperature (300 K). The hyperfine parameters for these complexes are presented in Table 3, and the spectra are shown in Figures 8 and S12, S13.

Neutral complexes **1** and **2** display a large "ferrocene-like" quadrupolar splitting, ΔE_q, characteristic of iron II (Fe^{2+}), and it was fitted to a single doublet associated with Fe^{2+}.

The spectrum of oxidized compound **1+** (Figure S13) presents a very weak signal. After 5 weeks, it was only possible to observe a small contribution consistent with Fe^{+3}, as expected after oxidation to one electron with ferricenium tetraborate.

Regarding the oxidized compound **2+**, the spectrum was fitted using two symmetrical doublets corresponding to the two-oxidation states (Fe^{2+} and Fe^{3+}). At 300 K, the resonant areas corresponding to Fe^{2+} (42%) and Fe^{3+} (58%) sites are akin, indicating that the chemical oxidation was produced in only one of the metallic centers (Figure 8 and Table 3). As was observed by Manriquez et al. and our research group,[49,50] a classical trapping ferrocene and ferrocenium center behavior at ambient temperature for the $[Cp^*Fe^{II}$-*as*-indaceneFe$^{III}Cp^*]^+$ and $[CpFe^{II}$-*p*-phenylene-Fe$^{III}Cp]^+$ compounds was evidenced, indicative of low electronic communication through the bridging ligand, different iron species derived from the fused ring ligand.[37,49]

In this context, the Mössbauer spectrum (for compound **2+**) and the cyclic voltammetry image for compound **2** suggest a low communication between the two ferrocenyl moieties; as mentioned by O'Hare et al.,[51] both techniques are appropriate to study electronic interactions because the values of ΔE_{ox} are close to zero or zero. On the other hand, for the monocation **2+**, Mössbauer investigation shows two symmetrical doublets corresponding two-oxidation states (Fe^{2+} and Fe^{3+}), meaning that the metals are noninteracting either because the ligand does not provide an electronic coupling pathway, as previously observed in other ferrocene-based 1,2,3-triazolyl derivatives[43,45] and as it is in our case for the bimetallic compound **2**.

https://doi.org/10.1021/acsomega.3c04996
ACS Omega 2023, 8, 35242−35255

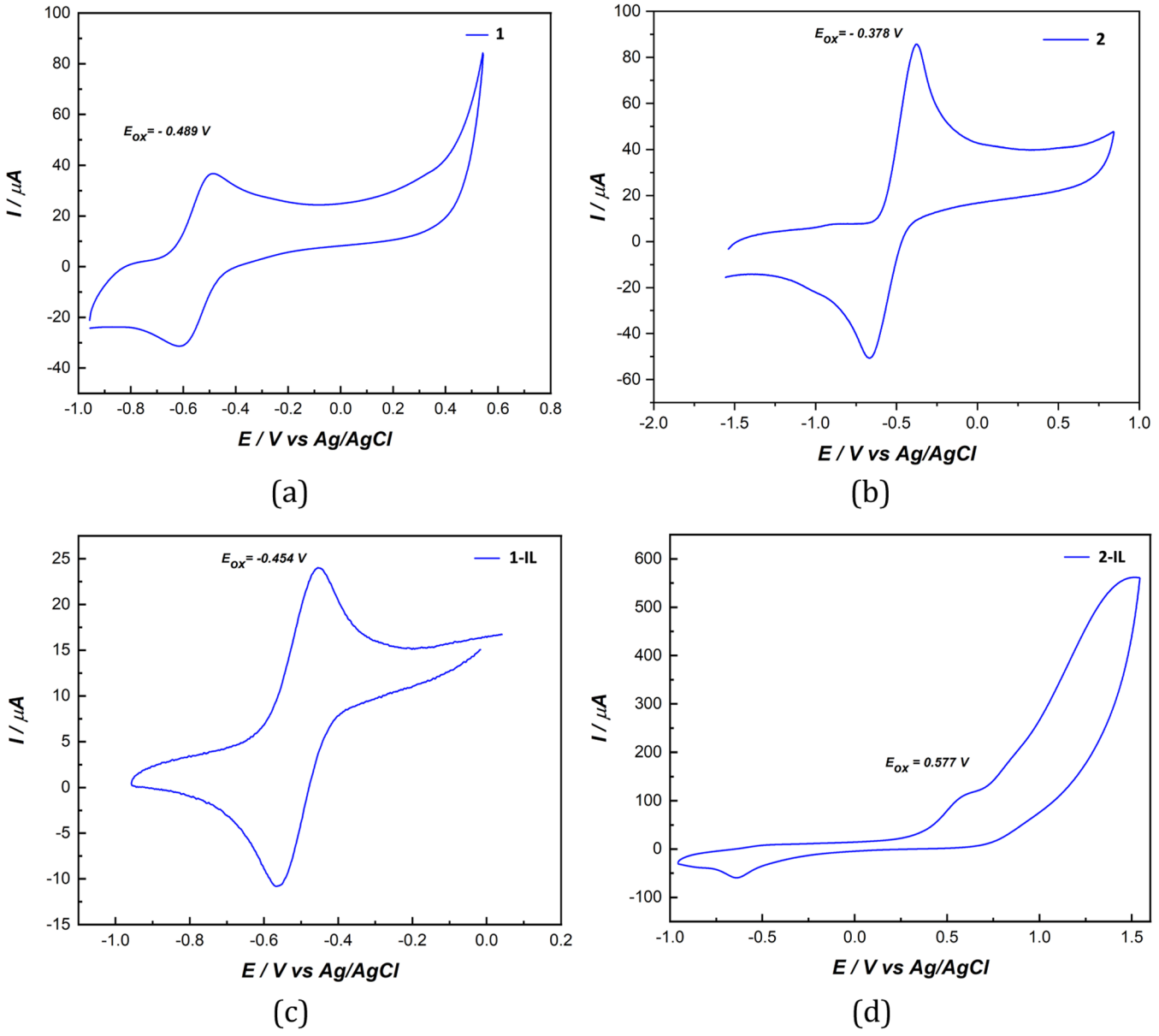

Figure 7. Cyclic voltammograms of complexes **1** (a), **2** (b), **1-IL** (c), and **2-IL** (c) in DMSO 0.1M *n*-Bu_4NBF_4. Scan rate 100 mV/s.

Table 3. Hyperfine Parameters for the Fitting of the Mössbauer Spectra at 300 K

compound		δ_{Fe} (mm s^{-1})	ΔE_q (mm s^{-1})	Γ (mm s^{-1})	area
1	Fe^{2+}	0.43(2)	2.32(4)	0.22(8)	1
1+	Fe^{3+}	0.43(7)	0.87(1)	0.31(2)	1
2	Fe^{2+}	0.44(3)	2.33(6)	0.24(8)	1
2+	Fe^{2+}	0.43(4)	2.37(8)	0.22(1)	0.42(2)
	Fe^{3+}	0.41(1)	0.67(2)	0.47(2)	0.58(2)

3.5. Antimigration Analysis. Composite solid-propellant samples were prepared to investigate the antimigration behavior of the burning rate catalysts **1**, **2**, **1-IL**, and **2-IL**. The details of the preparation of composite solid-propellant samples are shown in Table S1 of the Supporting Information.

Figure 9 shows the results of antimigration analyses. For these antimigration tests, ferrocene was used as a reference, exhibiting the highest migration with a value of 4.0 cm in 21 days; on long-term storage, ferrocene unavoidably moved the ends of the tube. Samples of compound **1** (MW:345.85 g/mol) and **2** (MW:608.31 g/mol) showed a lower antimigration behavior comparable with ferrocene and catocene, despite having a higher molecular weight (Figures 9, S14–S17). Compounds **1-IL** and **2-IL** have the best antimigration property among the samples due to their high molecular weights of 543.75 g/mol and 1009.50 g/mol, respectively. In general, the neutral compounds present lower antimigration behavior and the ionic derivatives present higher antimigration behavior, due not only because of their high molecular weight but also because they are ionic compounds, and they offer

https://doi.org/10.1021/acsomega.3c04996
ACS Omega 2023, 8, 35242−35255

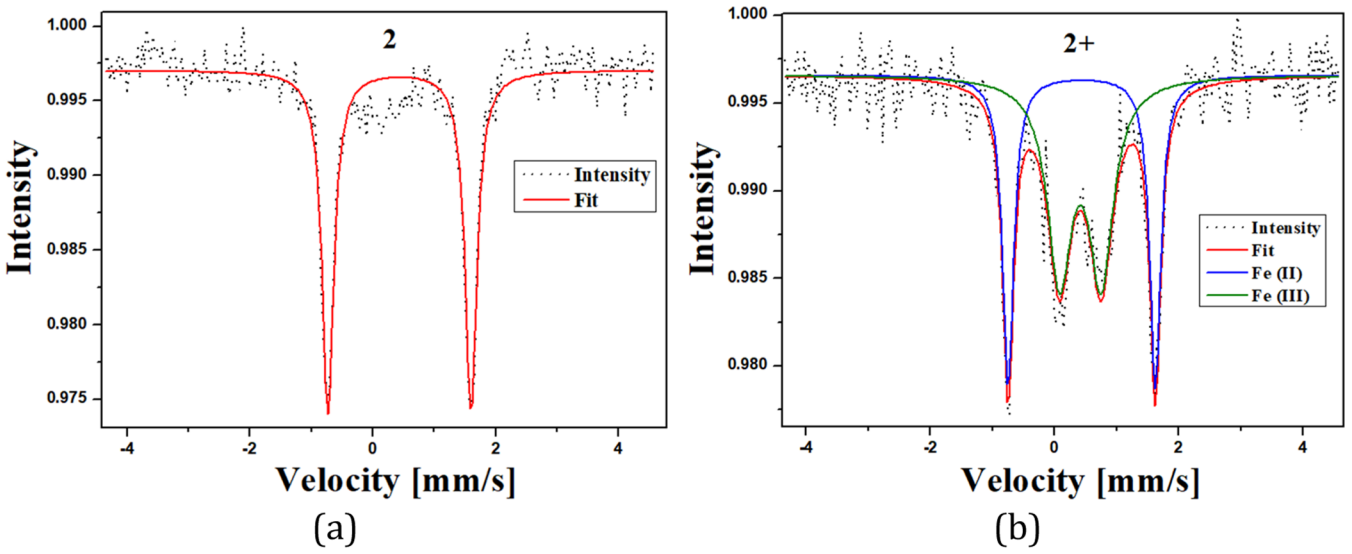

Figure 8. Mössbauer spectra of compound **2**,$[\{Cp_2Fe\}_2\text{-}Tr_2\text{-}Bz]^q$; q = 0 (a), +1 (b) at 300 K.

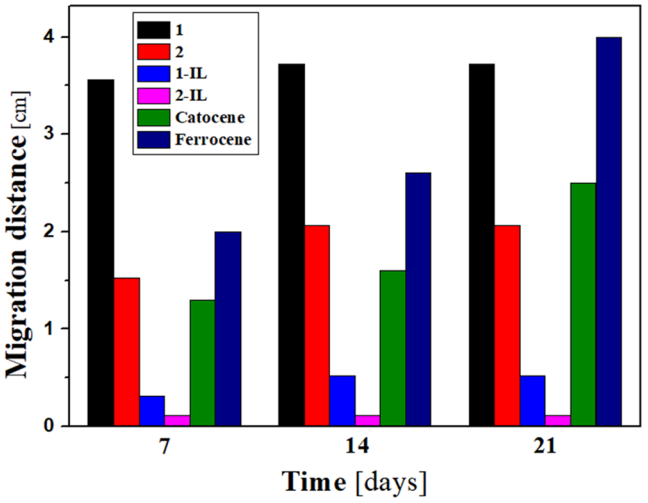

Figure 9. Evaluation of the migration tendency of **1**, **2**, **1-IL**, and **2-IL** along migration distance and for different aging times (the bars in each parallel row from left to right represent a compound that was aged for 7, 14, and 21 days, respectively, at 65 °C).

more significant electrostatic interaction with AP, the main component of the composite solid propellant. However, this force is not strong enough to prevent migration on long-time storage for compounds **1-IL** and **2-IL**.

3.6. Studies of Catalytic Effect on the Thermal Decomposition of Ammonium Perchlorate. A burning rate catalyst that demonstrates exceptional effectiveness requires specific thermal stability. Ammonium perchlorate is the primary oxidizer in composite solid propellants, and how it breaks down under heat significantly influences propellant combustion. The thermal stability of ferrocene-based 1,2,3-triazolyl compounds was assessed using the TG technique. As depicted in Figure S18, their weight loss began over 118 °C, except for compound **1-IL** (91.9 °C), obtaining a considerable loss of mass at the temperatures of 292, 318, 271, and 275 °C for compounds **1**, **2**, **1-IL**, and **2-IL**, respectively, highlighting their considerable resistance to high temperatures, suggesting that they are of high thermal stability, as was mentioned by Zhang and Zhao.[52−55]

Studies of the catalytic effect of the compounds **1**, **2**, **1-IL**, and **2-IL** on the thermal decomposition of AP were carried out by DSC. Figure 10 (Figures S19−S21 Supporting Information) shows the DSC curves of both AP and the mixture of AP with the related species and the weight percentages of these burning rate catalysts used in AP were 1, 3, and 5 wt %.

The combustion process of the solid-propellant rocket is closely related to AP's thermal decomposition temperature. The choice of a potential BR catalyst is attributed to shifting to the left the AP decomposition temperatures and high- and low-temperature decomposition (LTD and HTD). In addition, BR catalysts increase the heat released, contributing to higher energetic content in the propellants. All complexes here reported diminished thermal degradation temperature of AP, demonstrating its apparent catalytic effects.

The DSC curves of the thermal decomposition of AP show three processes, an endothermal and two exothermic processes. As is known, the orthorhombic to cubic crystal phase transition occurs at 248 °C and is associated with the endothermal peak.[8] The first exothermic process corresponds to the low-temperature decomposition (LTD) (292 °C), which is accepted by several authors to be associated with an electron transfer between ammonium and perchlorate ions, and the second exothermic peak is related to the high-temperature decomposition (HTD) step at 415 °C.[9]

The compounds **1**, **2**, **1-IL**, and **2-IL** as BR catalysts have a slight impact on the crystallographic transition temperature of AP during the endothermic phase transition process at 249 °C, as observed in previous work.[9,21,37]

All DSC curves showed similar AP decomposition profiles at different catalyst mass concentrations between the neutral compound and its ionic analogue, implying akin degradation mechanisms for the AP + ferrocene-based 1,2,3-triazolyl compound mixtures (Figures 10 and S19−S21). Multiple peaks within each DSC curve at 5%wt for complexes 1 and 1-IL suggest the potential existence of distinct decomposition mechanisms between the mixtures and the pure AP compared to complexes **2** and **2-IL**. It is possible to observe that for compounds **1**, **2**, and **1-IL**, there is a correlation between the increase in the percentage of the catalyst and its catalytic effect, obtaining the best catalytic performance at 5 wt %. About compound **2-IL**, its best catalytic effect was obtained at 3% by

https://doi.org/10.1021/acsomega.3c04996
ACS Omega 2023, 8, 35242−35255

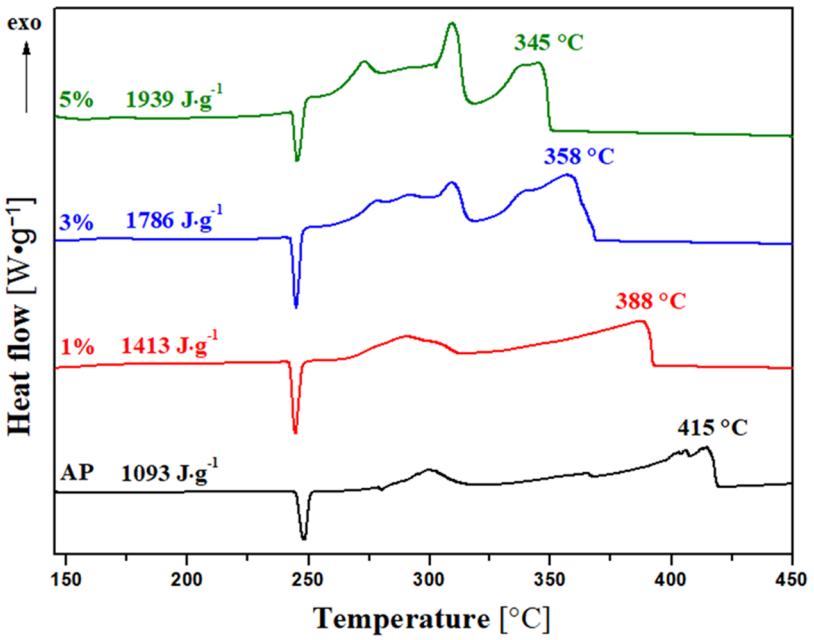

Figure 10. DSC curves for pure AP and a mixture of complex **1** with AP using different percentages (wt %).

Table 4. Summary of the Effect of the Different BR Catalysts (5 wt %) on the Thermal Decomposition of AP

compounds	E_{ox1} vs Ag/AgCl (mV)	HTD of AP (°C)	heat released (J·g^{-1})	heat released ratio[a]	nanoparticle size (nm)
NH_4ClO_4	825	415	1093	1	
Fc	500	360	1313	1.2	
1	−489	345	1939	1.8	8.8[b]
2	−378	361	1882	1.7	7.6[b]
1-IL	−454	366	1284	1.1	17.3[b]
2-IL	577	391	1350	1.2	15.0[b]
Cat[33]	346	346	2472	2.3	
Fe_2O_3[21]	−287	352	1839	1.7	
NP-Fe_2O_3		373	1447	1.3	30
NP-Fe_2O_3[63]		390	1244	1.1	3.5

[a]Ratio between the heat released by the mixture and the heat released by the neat AP. [b]Nanoparticles obtained in the catalytic tests.

weight since a retarding result is obtained at 5% by weight. Furthermore, all of the species reported here showed increased heat released in the 1284−1939 J·g^{-1} ranges compared to pure AP. It should be noted that the heat released by **1** (1939 J·g^{-1}) is higher than that released by the other species studied here but not comparable to the heat released from the catocene (Figure 10 and Table 4).

At 5 wt %, the diminutions of HTDs were 346, 361, 366, and 391 °C for **1**, **2**, **1-IL**, and **2-IL**, respectively, being 69, 54, 49, and 24 °C lower than the HTD for pure AP.

3.7. Possible Burning Rate Catalytic Mechanism. Ammonium perchlorate is a widely used oxidizer in solid rocket propellants due to its high oxygen balance and energy density.[8,56,57] However, its thermal decomposition is a complex and exothermic redox process that can pose safety hazards. As described in the introduction, to improve the performance and safety of AP-based propellants, various catalytic additives have been developed to modify the decomposition behavior of AP. In recent years, ferrocene has emerged as a promising class of catalysts for AP thermal decomposition. Understanding the catalytic mechanism of ferrocene is critical for its rational design and optimization.

Thus far, the commonly accepted substance as an intermediate in the degradation mechanism of AP through ferrocene derivatives has been identified as ferric oxide nanoparticles.[9] These nanoparticles are produced when the cyclopentadienyl ligand is separated from the iron atom and then oxidized to create nano-Fe_2O_3, which acts as a new catalyst to facilitate further decomposition of AP. However, there has not been any conclusive evidence of this phenomenon observed so far.

To elucidate the underlying reaction pathways, our research group took the residues from the pans after testing from the DSC and obtained the size of the nanostructures formed after thermal decomposition of AP determined by the TEM technique (Figures 11 and S22). In Figure 11a.1, the formation of two different nanostructures (spheres and rods) was observed for compound **1**. From this image, the histogram of Figure 11b.1 was generated, which allowed the determination of a diameter near 8.8 nm for the spherical nanoparticles. For compound **2**, in Figure 11a.2, only spherical nanostructures with a diameter close to 7.6 nm were observed. For compounds **1-IL** and **2-IL** (Figure S22), nanostructures with a spherical shape and sizes in the 15−17 nm range were determined.

These results agree with other authors' results in evaluating new catalysts for the thermal decomposition of AP[21,22,36,37,39]

https://doi.org/10.1021/acsomega.3c04996
ACS Omega 2023, 8, 35242−35255

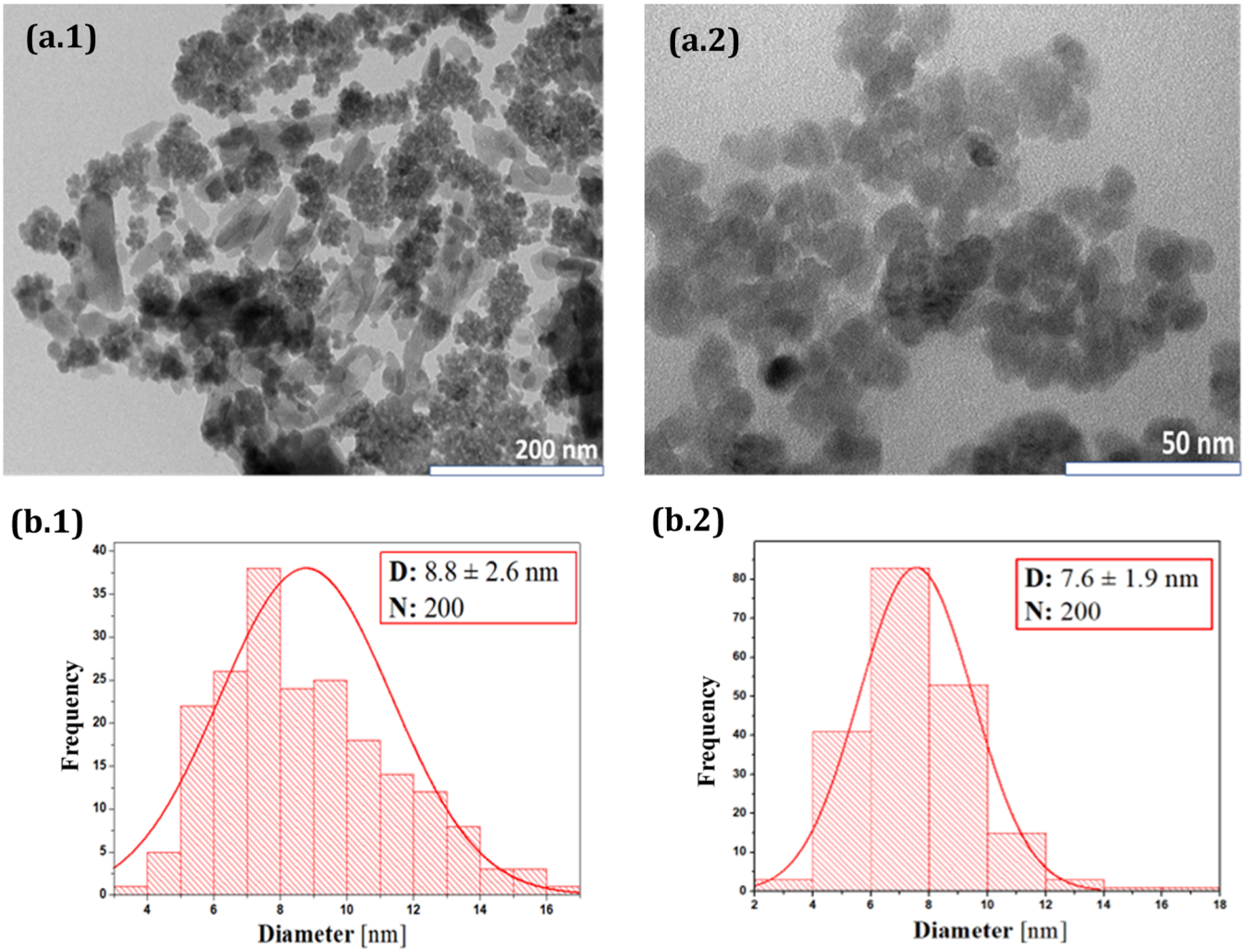

Figure 11. (a) TEM images and (b) histograms of compounds **1** and **2** after thermal degradation of AP.

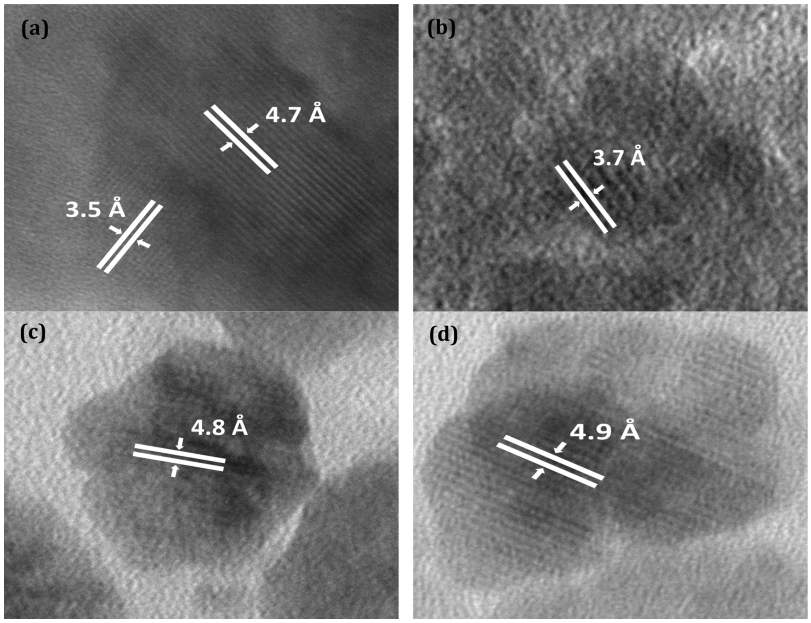

Figure 12. Magnified TEM images of the nanostructures produced by thermal degradation of AP with the compounds (a) **1**, (b) **2**, (c) **1-IL**, and (d) **2-IL**.

https://doi.org/10.1021/acsomega.3c04996
ACS Omega 2023, 8, 35242−35255

and with the obtention of nanoparticles from precursors derived from ferrocenes.[58,59]

Based on the selected area of TEM images (Figure S23), the lattice fringe analysis was carried out (Figure 12) to approach the possible species that make up the nanostructures produced in the thermal decomposition of AP. For compounds **1**, **1-IL**, and **2-IL**, a lattice fringe in the 4.7−4.9 Å range is observed, which could correspond to the (113) face of the maghemite.[58] Conversely, compounds **1** and **2** present a lattice fringe in the range of 3.5−3.7 Å, which could correspond to the (012) face of the hematite.[60] These lattice fringe values demonstrate nanoparticulate iron oxides' formation from the thermal decomposition of AP catalyzed with ferrocene-based 1,2,3-triazolyl compounds, as theoretically indicated by other authors in their studies.

In addition to TEM analyses, we perform an X-ray powder diffractogram (XRD) on the products after the catalysis of compound **1**. In this diffractogram, characteristic signals reported for derivatives of iron oxides, such as maghemite (Fe_2O_3) and hematite (Fe_3O_4), can be distinguished (Figure S24).[61,62] These results are consistent with those presented in Figures 12 and S23, allowing a preliminary identification of nanostructured iron oxides in the combustion product.

In this context, it is possible to analyze the relationship between the results previously obtained based on the different variables. Table 4 summarizes the oxidation potential, HTD, the heat released, and particle size formed after the thermal decomposition of the AP of the species reported here.

From Table 4, it is possible to observe two effects. The first effect corresponds to the exotherm's position depending greatly on the size of the Fe_2O_3 particles formed. As mentioned in the literature,[64] the catalytic activity of metal nanoparticles depends on their size and shape, which in turn are influenced by the method of preparation, and these shape-control and morphological studies of nanoparticles have attracted the attention of various investigators in the last few decades.[64−66] In our case, the presence of the butyl group in compounds **1-IL** and **2-IL** generates larger nanoparticles, double those caused by their analogues without N-alkylation, compounds **1** and **2**, which in turn leads to a decrease in the thermal catalytic effect on ammonium perchlorate and heat released.

The second effect is related to the oxidation potential; despite not observing a clear trend, it is possible to notice that compound **1** has a lower oxidation potential, which affects the process of the electron-transfer mechanism to the thermal decomposition of AP, generating a better catalytic effect and released heat. In contrast, compound **2-IL** has the lowest potential with a lower catalytic effect.

In this way, relating to a low oxidation potential, the formation of small nanoparticles, and an increase in the heat released, the mechanism of the catalytic effect on the thermal decomposition of ammonium perchlorate would be suggested as follows (Figure 13).

According to the traditional electron-transfer theory,[67] and according to our findings previously,[21,36,37] it is possible to indicate that systems with a reducing character promote electron transference plus the generation of Fe_2O_3 nanoparticles, which have a partially filled 3d orbit and provide help in an electro-transfer process. A positive hole within Fe_2O_3 enables it to receive electrons from an AP ion and its byproducts, thereby amplifying the process of thermal decomposition of AP. This effect is primarily attributed to the extensive surface area of nanostructured Fe_2O_3, which

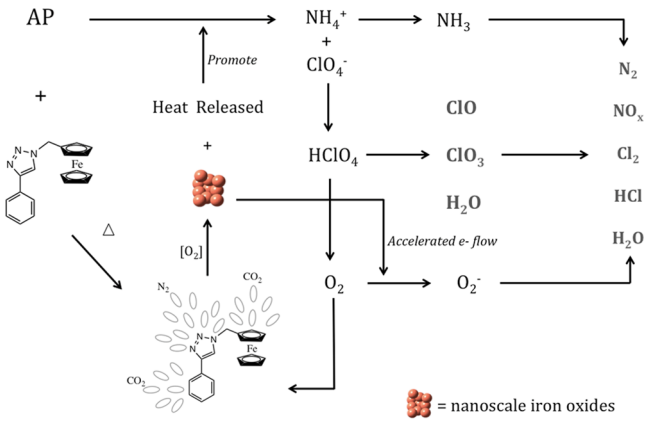

Figure 13. Proposed mechanism of AP's catalytic thermal degradation process through the decomposition of a ferrocene molecule (compound **1**) passing through the nanoparticulate ferric oxide intermediate.

creates numerous reactive sites on its surface. The atoms on the nanosized particles' surface exhibit higher reactivity than those in the bulk material, as they have fewer neighboring atoms and unoccupied sites.

Therefore, it is expected that these derivatives of ferrocene undergo AP decomposition via attack of the oxygen atom recently formed from the AP decomposition to form iron oxide nanoparticles.

The widely acknowledged mechanism for the electron-transfer decomposition of AP involves two key steps. First, an electron transfer between ClO_4^- and NH_4^+ ions forms NH_3 and $HClO_4$. Second, the oxygen (O_2) transforms superoxide (O_2^-) through a process generated from $HClO_4$ and subsequently converted to O_2^-. Ultimately, these ions, along with other gaseous byproducts, contribute to the decomposition of NH_3.

Thus, complex **1** has a much higher catalytic activity toward the thermal decomposition of AP than other species here reported and already published.

4. CONCLUSIONS

In conclusion, this study investigated the synthesis, characterization, and catalytic properties of mono- and bimetallic ferrocene-based 1,2,3-triazolyl compounds. The synthesis of the compounds was achieved through click reactions and N-alkylation reactions, with moderate to good yields (54−80%). The oxidation reactions produced oxidized compounds with good yields (68−78%). The complexes were characterized using NMR, FT-IR, and Mossbauer spectroscopies.

Furthermore, the redox properties of the complexes were investigated using cyclic voltammetry, which showed one quasireversible oxidation peak associated with the oxidation of the iron center. The oxidation potentials indicated the complexes' ability to undergo oxidation reactions, suggesting their potential as catalysts in the thermal decomposition of AP. Compound **1** is more active among the complexes here reported, shifting to the left the HTD of AP in 70 °C and increasing the heat released to 1939 $J \cdot g^{-1}$, at a rate 1.8 times higher than that of pure AP, but not comparable to the effect of catocene (2.3 ratio heat released).

Finally, postburning microscopy studies revealed evidence for the formation of iron nanoparticles, as mentioned by several authors, where particle sizes can be modulated through

https://doi.org/10.1021/acsomega.3c04996
ACS Omega 2023, 8, 35242−35255

alkylation of the triazolyl group, obtaining particle sizes in the range of 7−17 nm depending on the neutral or ionic catalyst used, which is closely related to the catalytic effect on the thermal decomposition of AP.

Overall, the synthesized ferrocene-type complexes exhibit promising characteristics for catalytic applications, potentially enhancing the thermal decomposition of AP. Further studies are warranted to explore their catalytic efficiency and performance in AP decomposition reactions, to develop effective catalysts for practical applications in solid propellants.

■ ASSOCIATED CONTENT

Supporting Information

The Supporting Information is available free of charge at https://pubs.acs.org/doi/10.1021/acsomega.3c04996.

NMR, FT-IR, Mössbauer characterization, migration analysis, TGA curves, and DSC curves to different wt % for all compounds (PDF)

■ AUTHOR INFORMATION

Corresponding Authors

Gabriel Abarca − *Universidad Bernardo OHiggins, Facultad de Ciencias de la Salud, Centro Integrativo de Biología y Química Aplicada (CIBQA), Santiago 8320000, Chile;* orcid.org/0000-0001-8477-2275; Email: gabriel.abarca@ubo.cl

Cesar Morales-Verdejo − *Universidad Bernardo OHiggins, Facultad de Ciencias de la Salud, Centro Integrativo de Biología y Química Aplicada (CIBQA), Santiago 8320000, Chile;* orcid.org/0000-0003-1706-3094; Email: cesar.morales@ubo.cl

Authors

Cristian Valdebenito − *Universidad Bernardo OHiggins, Facultad de Ciencias de la Salud, Centro Integrativo de Biología y Química Aplicada (CIBQA), Santiago 8320000, Chile*

José Gaete − *Universidad Bernardo OHiggins, Facultad de Ciencias de la Salud, Centro Integrativo de Biología y Química Aplicada (CIBQA), Santiago 8320000, Chile*

Claudio Osorio − *Universidad Bernardo OHiggins, Facultad de Ciencias de la Salud, Centro Integrativo de Biología y Química Aplicada (CIBQA), Santiago 8320000, Chile*

Yuvaraja Dibdalli − *Universidad Bernardo OHiggins, Facultad de Ciencias de la Salud, Centro Integrativo de Biología y Química Aplicada (CIBQA), Santiago 8320000, Chile*

Ángel Norambuena − *Laboratorio de Materiales Energéticos, Instituto de Investigaciones y Control del Ejército de Chile (IDIC), Santiago 8320000, Chile*

Nathalie Lecaros − *Centro de Estudios en Ciencia y Tecnología Militar, Academia Politécnica Militar (ACAPOMIL), Centro de Estudios en Ciencia y Tecnología de la Academia Politécnica Militar (CECTAP), Santiago 7850000, Chile*

Cristian Carrasco − *Centro de Estudios en Ciencia y Tecnología Militar, Academia Politécnica Militar (ACAPOMIL), Centro de Estudios en Ciencia y Tecnología de la Academia Politécnica Militar (CECTAP), Santiago 7850000, Chile*

Héctor Reyes − *Centro de Investigación e Innovación Tecnológica del Ejército de Chile (CIITEC), Santiago 7850000, Chile*

Complete contact information is available at: https://pubs.acs.org/10.1021/acsomega.3c04996

Author Contributions

C.V.: Formal analysis, methodology, and writing e review. **J.G.**: Formal analysis, investigation, writing e review, and editing. **C.O.**: Formal analysis and investigation. **Y.D.**: Formal analysis, writing e review & editing, and investigation. **A.N.**: Resources, formal analysis, investigation, writing e review, and editing. **N.L.**: Formal analysis, methodology, and investigation. **C.C.**: Formal analysis, methodology, and investigation. **H.R.**: Resources, formal analysis, and investigation. **G.A.**: Methodology, writing e review & editing, investigation, and supervision. **C.M.-V.**: Resources, conceptualization, methodology, writing e review & editing, investigation, and supervision.

Notes

The authors declare no competing financial interest.

■ ACKNOWLEDGMENTS

We gratefully acknowledge the financial support from FONDECYT grant 1210827 and Laboratory of Energy Materials from the Institute of Research and Control (IDIC) of the Chilean Army. The authors thank Professor Elies Molins and Dr. Ignasi Mata for their advice and discussion from Instituto de Ciencia de los Materiales de Barcelona (ICMAB-CSIC) for assistance with Mössbauer experiments.

■ REFERENCES

(1) Oehlschlaeger, M. A. Grand Challenges in Aerospace Propulsion. *Front. Aerosp. Eng.* **2022**, *1*, No. 1027943.

(2) Blakey-Milner, B.; Gradl, P.; Snedden, G.; Brooks, M.; Pitot, J.; Lopez, E.; Leary, M.; Berto, F.; du Plessis, A. Metal Additive Manufacturing in Aerospace: A Review. *Mater. Des.* **2021**, *209*, No. 110008.

(3) Agrawal, J. P. *High Energy Materials: Explosives, Propellants and Pyrotechnics*; WILEY-VCH, 2010.

(4) LING, W. Y. L.; Ling, L.; Zhang, S.; Fu, H.; Huang, M.; Quansah, J.; Liu, X.; Wang, N. A Brief Review of Alternative Propellants and Requirements for Pulsed Plasma Thrusters in Micropropulsion Applications. *Chin. J. Aeronaut.* **2020**, *33*, 2999−3010.

(5) Gao, Y.; Liu, Y.; Ma, D. Effect of Operation Pressure on Heat Release Characteristics in Solid Rocket Motor Nozzle Considering Detailed Chemical Reaction Mechanism. *Aerosp. Sci. Technol.* **2022**, *128*, No. 107794.

(6) Chaturvedi, S.; Dave, P. N. Solid Propellants: AP/HTPB Composite Propellants. *Arabian J. Chem.* **2019**, *12*, 2061−2068.

(7) Norambuena, Á.; Gutiérrez, P.; Arroyo, J. L.; Reyes, H.; Morales-verdejo, C. Studies of Burning Rate and Pressure Exponent of a New Combustion Catalyst Derived from P-Phenylene. *J. Energy Mater.* **2023**, *41*, 157−170.

(8) Boldyrev, V. V. Thermal Decomposition of Ammonium Perchlorate. *Thermochim. Acta* **2006**, *443*, 1−36.

(9) Liu, J.; Yu, H.; Wang, L.; Vatsadze, S. Z.; Huang, Z.; Ul, B. A Review on Synthesis of Fe-Based Compounds and Their Properties as the Burning Rate Catalysts for Propellants. *J. Organomet. Chem.* **2022**, *980−981*, No. 122514.

(10) Kishore, K.; Sunitha, M. R. Mechanism of Catalytic Activity of Transition Metal Oxides on Solid Propellant Burning Rate. *Combust. Flame* **1978**, *33*, 311−314.

(11) Maggi, F.; Dossi, S.; Paravan, C.; Galfetti, L.; Rota, R.; Cianfanelli, S.; Marra, G. Iron Oxide as Solid Propellant Catalyst: A Detailed Characterization. *Acta Astronaut.* **2019**, *158*, 416−424.
(12) Gaete, J.; Arroyo, J. L.; Norambuena, A.; Abarca, G.; Morales-verdejo, C. Mechanistic Insights into the Thermal Decomposition of Ammonium Perchlorate: The Role of Amino-Functionalized Magnetic Nanoparticles. *Inorg. Chem.* **2022**, *61*, 1447−1455.
(13) Gaete, J.; Valdebenito, C.; Dibdalli, Y.; Arroyo, J. L.; Norambuena, Á.; Valenzuela, F.; Basualto, C.; Abarca, G.; Morales-Verdejo, C. Superparamagnetic Energetic Nanoparticles: A Surface Self- Propagation Pathway for the Thermal Decomposition of Ammonium Perchlorate. *J. Therm. Anal. Calorim.* **2023**, *148*, 2313−2321.
(14) Lin, H.; Zhang, Q.; Liu, H.; Shen, S.; Guo, Z.; Jin, B.; Peng, R. Understanding the Synergistically Enhanced Thermocatalytic Decomposition of Ammonium Perchlorate Using Cobalt Nanoparticle-Embedded. *Mater. Adv.* **2023**, *4*, 2332−2339.
(15) Chaturvedi, S.; Dave, P. N. A Review on the Use of Nanometals as Catalysts for the Thermal Decomposition of Ammonium Perchlorate. *J. Saudi Chem. Soc.* **2013**, *17*, 135−149.
(16) Dave, P. N.; Sirach, R. Graophene Oxide Based Nickel-Copper and Copper − Zinc Cobaltite: Catalysts for the Thermolysis of Ammonium Perchlorate and Nitrotriazolone. *Energy Adv.* **2023**, *2*, 679−690.
(17) Wang, J.-S.; Liu, Y.; Zhao, H.; Liu, J.; Wang, D.; Song, Y.; Wang, Y. Metal Compound-Enhanced Flame Retardancy of Intumescent Epoxy Resins Containing Ammonium Polyphosphate. *Polym. Degrad. Stab.* **2009**, *94*, 625−631.
(18) Xu, Y.; Wang, Y.; Zhong, Y.; Lei, G.; Li, Z.; Zhang, J.; Zhang, T. Transition Metal Complexes Based on Hypergolic Anions for Catalysis of Ammonium Perchlorate Thermal Decomposition. *Energy Fuels* **2020**, *34*, 14667.
(19) Escobar, M. A.; Morales-Verdejo, C.; Arroyo, J. L.; Dreyse, P.; González, I.; Brito, I.; MacLeod-Carey, D.; Moreno da Costa, D.; Cabrera, A. R. Burning Rate Performance Study of Ammonium Perchlorate Catalyzed by Heteroleptic Copper(I) Complexes with Pyrazino[2,3-f][1,10]Phenanthroline-Based Ligands. *Eur. J. Inorg. Chem.* **2021**, *2021*, 1632−1639.
(20) Moreno da Costa, D.; Henriquez, M. A.; Gonzalez-Torres, D.; Zuñiga-Loyola, C.; Brito, I.; Gonzalez, I.; Villegas-Menares, A.; Macleod-Carey, D.; Morales-verdejo, C.; Cabrera, A. R. Influence of the Thermal Stability of Ammonium Perchlorate in Presence of Heteroleptic Copper (I) Complexes Bearing Ethane-1,2-Diimine and Biphosphines. *Inorg. Chim. Acta* **2023**, *545*, No. 121249.
(21) Arroyo, J. L.; Norambuena, A.; Reyes, H.; Valdebenito, C.; Abarca, G.; Carey, D. M.; Morales-verdejo, C. Heterobimetallic Catalysts for the Thermal Decomposition of Ammonium Perchlorate: Efficient Burning Rate Catalysts for Solid Rocket Motors and Missiles. *Inorg. Chem.* **2021**, *60*, 1436−1448.
(22) Ríos, P. L.; Araya-Durán, I.; Bonardd, S.; Arroyo, J. L.; Povea, P.; Camarada, M. B. Ferrocene-Modified Dendrimers as Support of Copper Nanoparticles: Evaluation of the Catalytic Activity for the Decomposition of Ammonium Perchlorate. *Mater. Today Chem.* **2022**, *23*, No. 100631.
(23) Qasem, A.; Zhang, X.; Xie, Z.; Zhang, Q.; Sun, H.; Gao, Z.; Yang, J.; Khan, H.; Zhang, W.; Hu, B.; Zhang, G. Triazine-Augmented Catalytic Activity of Cyclobutadiene Tricarbonyl Fe(0) Complexes for Thermal Decomposition of Ammonium Perchlorate. *Organometallics* **2023**, *42*, 384−391.
(24) Zhao, Y.; Hou, Y.; Xu, Z.; Chang, S.; Gou, X.; Zhao, J. Synthesis and Properties of Binuclear Ferrocene Energetic Compounds as Combustion Rate Catalyst. *Z. Anorg. Allg. Chem.* **2022**, *648*, No. e202200075.
(25) Cheng, W.; Shi, X.; Zhang, Y.; Jian, Y.; Zhang, G. Novel Ferrocene-Based 1,2,3-Triazolyl Compounds: Synthesis, Anti-Migration Properties and Catalytic Effects on Oxidizers during Combustion. *Inorg. Chim. Acta* **2020**, *502*, No. 119374.
(26) Guo, H.; Huo, D.; Zhao, H.; Chen, S. Synthesis, Anti-Migration and Catalytic Effect of Ferrocene Azine Derivatives on the Thermal Decomposition of Ammonia Perchlorate. *Z. Anorg. Allg. Chem.* **2022**, *648*, No. e202200053.
(27) Shi, X.; Yang, L.; Jiang, L.; Bi, F.; Zhang, G. Anti-Migration of Nitrogen-Rich N-Heterocyclic Ferrocenes and Their Combustion Catalytic Properties in the Thermal Decomposition of Energetic Oxidizers. *Z. Anorg. Allg. Chem.* **2022**, *648*, No. e202100324.
(28) Amin, B. U.; Yu, H.; Wang, L.; Nazir, A.; Fahad, S.; Haq, F.; Mahmood, S.; Liang, R.; Uddin, A.; Lin, T. Recent Advances on Ferrocene-Based Compounds and Polymers as a Burning Rate Catalysts for Propellants. *J. Organomet. Chem.* **2020**, *921*, No. 121368.
(29) Gao, J.; Wang, L.; Tai, Y.-L.; Wang, J.; Huo, J.; Amin; Abid Muhammad Haojie, Y.; Ding, W. Study on Poly(Ferrocenylsilane) and Its Promotive Effect to Decomposition of Ammonium Perchlorate. *J. Propul. Power* **2011**, *27*, 1143−1145.
(30) Deng, Z.; Yu, H.; Wang, L.; Zhai, X.; Chen, Y.; Sun, R. Synthesis of Ferrocenyl Functionalized Hyperbranched Polyethylene and Its Application as Low Migration Burning Rate Catalyst. *J. Organomet. Chem.* **2015**, *799*−*800*, 273−280.
(31) Zain-ul-Abdin; Wang, L.; Yu, H.; Saleem, M.; Akram, M.; Abbasi, N. M.; Khalid, H.; Sun, R.; Chen, Y. Ferrocene-Based Polyethyleneimines for Burning Rate Catalysts. *New J. Chem.* **2016**, *40*, 3155−3163.
(32) Jiang, L.; Liu, M.; Xu, L.; Dong, T.; Li, J.; Zhang, G. Synthesis and Characterization of a Dinuclear Nitrogen-Rich Ferrocenyl Ligand and Its Ionic Coordination Compounds and Their Catalytic Effects During Combustion. *Z. Anorg. Allg. Chem.* **2019**, *645*, 92−100.
(33) Cheng, Z.; Zhang, G.; Fan, X.; Bi, F.; Zhao, F.; Zhang, W.; Gao, Z. Synthesis, Characterization, Migration and Catalytic Effects of Energetic Ionic Ferrocene Compounds on Thermal Decomposition of Main Components of Solid Propellants. *Inorg. Chim. Acta* **2014**, *421*, 191−199.
(34) Liu, X.; Zhao, D.; Bi, F.; Fan, X.; Zhao, F.; Zhang, G.; Zhang, W.; Gao, Z. Synthesis, Characterization, Migration Studies and Combustion Catalytic Performances of Energetic Ionic Binuclear Ferrocene Compounds. *J. Organomet. Chem.* **2014**, *762*, 1−8.
(35) Morales-Verdejo, C.; Camarada, M. B.; Arroyo, J. L.; Povea, P.; Carreño, G.; Manriquez, J. M. Effect of the Homo- and Heterobimetallic Compounds Derived from s-Indacene on the Thermal Decomposition of Ammonium Perchlorate: Potential Applications as Burning Rate Catalysts. *J. Therm. Anal. Calorim.* **2018**, *131*, 353−361.
(36) Povea, P.; Arroyo, J. L.; Carreño, G.; Norambuena, Á.; Rios, P. L.; Camarada, M. B.; Chavez, I.; Manriquez, J. M.; Morales-Verdejo, C. Catalytic Effects of P-Phenylene-Bridged Methylated Binuclear Ferrocenes on Thermal Decomposition of the Main Component of Composite Solid Propellants. *Thermochim. Acta* **2018**, *666*, 181−189.
(37) Arroyo, J. L.; Povea, P.; Faúndez, R.; Camarada, M. B.; Cerda-cavieres, C.; Abarca, G.; Manriquez, J. M.; Morales-Verdejo, C. Influence Iron-Iron Distance on the Thermal Decomposition of Ammonium Perchlorate. New Catalysts for the Highly Efficient Combustion of Solid Rocket Propellant. *J. Organomet. Chem.* **2020**, *905*, No. 121020.
(38) Shi, X.; Cheng, W.; Jiang, L.; Bi, F.; Li, J.; Zhang, G. Anti-Migration and Combustion Catalytic Performances of Ferrocenyl Compounds of Anilines and Alkylamines Synthesized by Click Reaction. *Z. Anorg. Allg. Chem.* **2021**, *647*, 463−470.
(39) Liu, X.; Feng, H.; Li, Y.; Ma, X.; Chen, F.; Yan, Q. Ferrocene-Based Hydrazone Energetic Transition-Metal Complexes as Multifunctional Combustion Catalysts for the Thermal Decomposition of Ammonium Perchlorate. *J. Ind. Eng. Chem.* **2022**, *115*, 193−208.
(40) Chai, C. L. L.; Armarego, W. L. F. *Purification of Laboratory Chemicals*, 5th ed.; Butterworth-Heinemann: Oxford, 2003.
(41) Ciampi, S.; Eggers, P. K.; Saux, G.; Le James, M.; Harper, J. B.; Gooding, J. J. Silicon (100) Electrodes Resistant to Oxidation in Aqueous Solutions: An Unexpected Benefit of Surface Acetylene Moieties. *Langmuir* **2009**, *25*, 2530−2539.
(42) Telegina, L. N.; Kelbysheva, E. S.; Strelkova, T. V.; Ezernitskaya, M. G.; Borisov, Y. A.; Smol'yakov, A. F.; Peregudov, A. S.; Rodionov, A. N.; Ikonnikov, N. S.; Loim, N. M. Transalkylation

https://doi.org/10.1021/acsomega.3c04996
ACS Omega 2023, 8, 35242−35255

and Migration of N-Substituent upon Alkylation of 1,2,3-Triazoles Containing Good Leaving N-Substituents. *Eur. J. Org. Chem.* **2016**, *2016*, 5897−5906.
(43) Badèche, S.; Daran, J.-C.; Ruiz, J.; Astruc, D. Synthesis and Coordination Chemistry of Ferrocenyl-1,2,3-Triazolyl Ligands. *Inorg. Chem.* **2008**, *47*, 4903−4908.
(44) Kowalski, K. A Brief Survey on the Application of Metal-Catalyzed Azide−Alkyne Cycloaddition Reactions to the Synthesis of Ferrocenyl-x-1,2,3-Triazolyl-R (x = None or a Linker and R = Organic Entity) Compounds with Anticancer Activity. *Coord. Chem. Rev.* **2023**, *479*, No. 214996.
(45) Rajakumar, P.; Kannan, A.; Anandhan, R. Synthesis, Photophysical and Electrochemical Properties of 1,2,3-Triazolyl Bridged Ferrocenyl Dendrimers through Click Chemistry. *New J. Chem.* **2014**, *38*, 1594.
(46) Telegina, L. N.; Kelbysheva, E. S.; Strelkova, T. V.; Ezernitskaya, M. G.; Borisov, Y. A.; Smol'yakov, A. F.; Peregudov, A. S.; Rodionov, A. N.; Ikonnikov, N. S.; Loim, N. M. Transalkylation and Migration of *N* -Substituent upon Alkylation of 1,2,3-Triazoles Containing Good Leaving *N* -Substituents. *Eur. J. Org. Chem.* **2016**, *2016*, 5897−5906.
(47) Xiang, J.; Burges, R.; Häupler, B.; Wild, A.; Schubert, U. S.; Ho, C.-L.; Wong, W.-Y. Synthesis, Characterization and Charge−Discharge Studies of Ferrocene-Containing Poly-(Fluorenylethynylene) Derivatives as Organic Cathode Materials. *Polymer* **2015**, *68*, 328−334.
(48) Valizadeh, H.; Amiri, M.; Khalili, E. Task-Specific Nitrite and Azide Ionic Liquids for the Efficient One-Pot Synthesis of 1,2,3-Triazoles from the Aniline Derivatives. *Mol. Diversity* **2012**, *16*, 319−323.
(49) Manriquez, J. M.; Ward, M. D.; Reiff, W. M.; Calabrese, J. C.; Jones, N. L.; Carroll, P. J.; Bunel, E. E.; Miller, J. S. Structural and Physical Properties of Delocalized Mixed-Valent [Cp*M(Pentalene)-M'Cp*]N+ and [Cp*M(Indacene)M'Cp*]N+ (M, M' = Fe, Co, Ni; n = 0, 1, 2) Complexes. *J. Am. Chem. Soc.* **1995**, *117*, 6182−6193.
(50) Dibdalli, Y.; Valdebenito, C.; Amshumali, M. K.; Molins, E.; Morales-verdejo, C. An Improved Synthesis of P -Phenylene-Bridged Methylated Binuclear Ferrocene. *J. Chil. Chem. Soc.* **2022**, *67*, 5414−5417.
(51) Aguirre-Etcheverry, P.; O'Hare, D. Electronic Communication through Unsaturated Hydrocarbon Bridges in Homobimetallic Organometallic Complexes. *Chem. Rev.* **2010**, *110*, 4839−4864.
(52) Li, J.; Gao, X.; Shao, E.; Zhang, G. Synthesis, Characterization and Migration of Ionic Polyferrocenyl Compounds of 5-Ferrocenyl-1H-Tetrazole and Their Effects During Combustion. *Z. Anorg. Allg. Chem.* **2017**, *643*, 455−463.
(53) Guo, H.; Huo, D.; Zhao, H.; Chen, S. Synthesis, Anti-migration and Catalytic Effect of Ferrocene Azine Derivatives on the Thermal Decomposition of Ammonia Perchlorate. *Z. Anorg. Allg. Chem.* **2022**, *648*, No. e202200053.
(54) Jiang, L.; Liu, M.; Xu, L.; Dong, T.; Li, J.; Zhang, G. Synthesis and Characterization of a Dinuclear Nitrogen-Rich Ferrocenyl Ligand and Its Ionic Coordination Compounds and Their Catalytic Effects During Combustion. *Z. Anorg. Allg. Chem.* **2019**, *645*, 92−100.
(55) Li, J.; Jiang, L.; Jia, D.; Xu, L.; Zhang, G. Ferrocenyl Ionic Compounds Containing [Fe(CN) 6] 3- Anions: Synthesis, Characterization, and Catalytic Effects during Combustion. *Z. Anorg. Allg. Chem.* **2019**, *645*, 14−21.
(56) Shen, S. M.; Chen, S. I.; W, B. B. The Thermal Decomposition of Ammonium Perchlorate (AP). Containing a Burning Rate Modifier. *Thermochim. Acta* **1993**, *223*, 135−143.
(57) Mahinroosta, M. Catalytic Effect of Commercial Nano-CuO and Nano-Fe2O3 on Thermal Decomposition of Ammonium Perchlorate. *J. Nanostruct. Chem.* **2013**, *3*, No. 47.
(58) Bhalerao, G. M.; Sinha, A. K.; Srivastava, H.; Srivastava, A. K. Synthesis and Studies of Growth Kinetics of Monodispersed Iron Oxide Nanoparticles Using Ferrocene as Novel Precursor. *Appl. Phys. A* **2009**, *95*, 373−380.
(59) Amara, D.; Grinblat, J.; Margel, S. Solventless Thermal Decomposition of Ferrocene as a New Approach for One-Step Synthesis of Magnetite Nanocubes and Nanospheres. *J. Mater. Chem.* **2012**, *22*, 2188−2195.
(60) Khalil, M.; Yu, J.; Liu, N.; Lee, R. L. Hydrothermal Synthesis, Characterization, and Growth Mechanism of Hematite Nanoparticles. *J. Nanopart. Res.* **2014**, *16*, No. 2362.
(61) Niederberger, M.; Krumeich, F.; Hegetschweiler, K.; Nesper, R. An Iron Polyolate Complex as a Precursor for the Controlled Synthesis of Monodispersed Iron Oxide Colloids. *Chem. Mater.* **2002**, *14*, 78−82.
(62) Kim, W.; Suh, C.-Y.; Cho, S.-W.; Roh, K.-M.; Kwon, H.; Song, K.; Shon, I.-J. A New Method for the Identification and Quantification of Magnetite−Maghemite Mixture Using Conventional X-Ray Diffraction Technique. *Talanta* **2012**, *94*, 348−352.
(63) Joshi, S. S.; Patil, P. R.; Krishnamurthy, V. N. Thermal Decomposition of Ammonium Perchlorate in the Presence of Nanosized Ferric Oxide. *Def. Sci. J.* **2008**, *58*, 721−727.
(64) Telkar, M. M.; Rode, C. V.; Chaudhari, R. V.; Joshi, S. S.; Nalawade, A. M. Shape-Controlled Preparation and Catalytic Activity of Metal Nanoparticles for Hydrogenation of 2-Butyne-1,4-Diol and Styrene Oxide. *Appl. Catal., A* **2004**, *273*, 11−19.
(65) Peng, X.; Manna, L.; Yang, W.; Wickham, J.; Scher, E.; Kadavanich, A.; Alivisatos, A. P. Shape Control of CdSe Nanocrystals. *Nature* **2000**, *404*, 59−61.
(66) Seitkalieva, M. M.; Samoylenko, D. E.; Lotsman, K. A.; Rodygin, K. S.; Ananikov, V. P. Metal Nanoparticles in Ionic Liquids: Synthesis and Catalytic Applications. *Coord. Chem. Rev.* **2021**, *445*, No. 213982.
(67) Kumar, H.; Tengli, P. N.; Mishra, V. K.; Tripathi, P.; Bhushan, A.; Mishra, P. K. The Effect of Reduced Graphene Oxide on the Catalytic Activity of Cu−Cr−O−TiO2 to Enhance the Thermal Decomposition Rate of Ammonium Perchlorate: An Efficient Fuel Oxidizer for Solid Rocket Motors and Missiles. *RSC Adv.* **2017**, *7*, 36594−36604.

https://doi.org/10.1021/acsomega.3c04996
ACS Omega 2023, 8, 35242−35255